Fractional-order controllers for irrational systems

Guel-Cortez, A-J., Mendez-Barrios, C-F., Kim, E. & Sen, M.

IET Control Theory & Applications

The Institution of Engineering and Technology WILEY

ORIGINAL RESEARCH PAPER

Fractional-order controllers for irrational systems

Adrian-Josue Guel-Cortez[1] ⓘ | **César-Fernando Méndez-Barrios[2]** | **Eun-jin Kim[1]** | **Mihir Sen[3]**

[1] Centre for Fluid and Complex Systems, Coventry University, Priory Street, Coventry CV1 5FB, UK

[2] Facultad de Ingeniería, Universidad Autónoma de San Luis Potosí (UASLP), Dr. Manuel Nava No. 8, San Luis Potosí, México

[3] Department of Aerospace & Mechanical Engineering, University of Notre Dame, Notre Dame, IN 46556, USA

Correspondence
Adrian-Josue Guel-Cortez, Centre for Fluid and Complex Systems, Coventry University, Priory Street CV1 5FB, Coventry, UK.
Email: guelcortea@uni.coventry.ac.uk

Funding information
Centre for Fluid and Complex Systems; CONACyT-Mexico; Leverhulme Trust, Grant/Award Number: RF- 2018-142-9

Abstract
In this contribution, fractional-order controllers of the type PD^μ and PI^λ are applied to a class of irrational transfer function models that appear in large-scale systems, such as networks of mechanical/electrical elements and distributed parameter systems. More precisely, by considering the fractional-order controller $k_p + k_\eta s^\alpha$ in the Laplace domain with $-1 \leq \alpha \leq 1$, a stability analysis in the parameter-space (k_p, k_η, α) is presented. Furthermore, as a way to measure the controller robustness, the controller's fragility analysis using the parameter-space (k_p, k_η, α) is derived. Finally, several applications that demonstrate the utility of our results are included.

1 | INTRODUCTION

Irrational systems (ISs) are a class of systems whose model is represented by a transfer function containing irrational orders. In [1, 2] ISs are described as implicit operators because they are solutions to an operator equation. Besides, [3] presents ISs as a type of pseudo-differential time-operators whose representation in time domain is diffusive (for further details about the diffusive representation, see ref. [4]). Practical examples of ISs can be found in various previous works across different disciplines. For instance, [2] introduces an IS model to represent the total operator describing the potential-driven flow dynamics in a large-scale self-similar tree network. In references [5–7], a version with springs and dampers of this IS is examined to propose model reductions to robotic formations or cyber-physical systems. On the other hand, infinite ladder networks can also be modelled by using an IS representation (for further details, see ref. [1]). In his famous text [8], Richard Feynman studies an infinite LC ladder circuit and proposes an expression for its total impedance in the form of an IS. Recently, this model is examined in more detail in ref. [9]. In ref. [10], an IS model for

an infinite ladder of mass-springs and dampers is introduced towards the goal of modelling complex networks of mechanical systems. Furthermore, to describe the power-law behaviour in soft tissue, a hierarchical fractal ladder network model is proposed in [11]. Finally, ISs can also be found when solving partial differential equations or when modelling distributed parameter systems (for further details, see refs. [12–14]).

As it can be seen from the previous discussion, ISs arise as an approximation, model reduction or exact model for certain complex or large-scale systems [5]. Regarding the design of control strategies for complex systems, many solutions have been proposed in the literature (see, for instance, refs. [15–19]), but for the case of ISs, it still remains as an open problem. Thus, by considering the benefits that ISs can bring to the modelling of complex systems, it will be of core importance to study control schemes for these mathematical models. Between the most popular control techniques, there is the well-known PID controller whose "popularity" can be attributed to its particular distinct features: simplicity and ease of implementation. In this regard, inspired by its attributes as well as the recent developments in fractional calculus, a fractional-order version of the

classical PID has raised the attention of different researchers (see, for instance, refs. [20–26]). These fractional-order PID or $\mathrm{PI}^{\lambda}\mathrm{D}^{\mu}$ controllers include a derivative D^{μ} and an integral I^{λ} of non-integer orders $\mu, \lambda > 0 \in \mathbb{R}$. The values μ and λ add more degrees of freedom to the controller, which creates a more flexible controller in comparison with the classical PID controller [27]. In addition, in the work of Podlubny [28], it has been shown that $\mathrm{PI}^{\lambda}\mathrm{D}^{\mu}$ controllers provide better results when being applied to fractional-order systems. Therefore, because ISs are a type of fractional-order systems [2, 10], fractional-order controllers are the most suitable option to control ISs. In general, fractional-order systems' stability and fractional-order PID controllers's design have been already studied for different applications, for some examples, see refs. [22, 29–35]. More precisely for the case of ISs, in the previous work [36], we have introduced the design of fractional PD^{μ} controllers for ISs without analysing the effects of changing the controller's parameter μ to find the stability in the (k_p, k_{η}, μ) parameter-space.

An important aspect to consider when designing any type of controllers is the fragility analysis. Roughly speaking, a controller for which the closed-loop system is destabilised by small perturbations in the controller parameters is called "fragile" [37]. Among various reasons to study the controller's fragility, one of the most important tasks to be considered is the fact that every controller implementation is subject to the imprecision inherent in analogue–digital and digital–analogue conversion, finite word length, finite resolution measuring instruments and round-off errors in numerical computations [38–40].

With the above background as a motivation, the aim of this paper is to present a procedure to design non-fragile stabilising fractional-order controllers of PD^{μ} and PI^{λ}-type to a class of ISs. Such an analysis will be performed by means of the D-composition method [41, 42] to obtain the parameter-space (k_p, k_{η}, α), where k_p, k_{η} and $\alpha \in [-\lambda, \mu]$ represent the control parameters that bounded-input, bounded-output (BIBO) stabilise the IS and by computing the controller's fragility in the parameter-space (k_p, k_{η}, α).

The remainder of the paper is organised as follows: Section 2 reviews the fundamental concepts and preliminary results that will be used throughout the paper, and formulates the main problems to be solved. In Section 3, we present our controller restrictions, the characterisation of the stability crossing boundaries, the crossing direction analysis and the fragility analysis to solve the described problems. In Section 4, we analyse several specific examples to show the effectiveness and applicability of the theory. Finally, Section 5, contains some concluding remarks.

The notation used through the paper is as follows: $\mathbb{C}$ is the set of complex numbers, $i := \sqrt{-1}$, all points in the complex plane whose real parts are positive, will be called the right half-plane (RHP), whereas all points whose real part are negative will be called the left half-plane (LHP). $\mathbb{C}_+$ and $\mathbb{C}_-$ stand for the closed RHP and the open RHP of the first Riemann sheet, respectively. Also, for $z \in \mathbb{C}$, $\bar{z}$, $\arg z$, $\mathfrak{R}\{z\}$ and $\mathfrak{I}\{z\}$ define the complex conjugate, main argument (i.e. $\arg z \in (-\pi, \pi]$), and the real and imaginary parts of z respectively. $\mathbb{R}$ ($\mathbb{R}_+$ and $\mathbb{R}_-$)
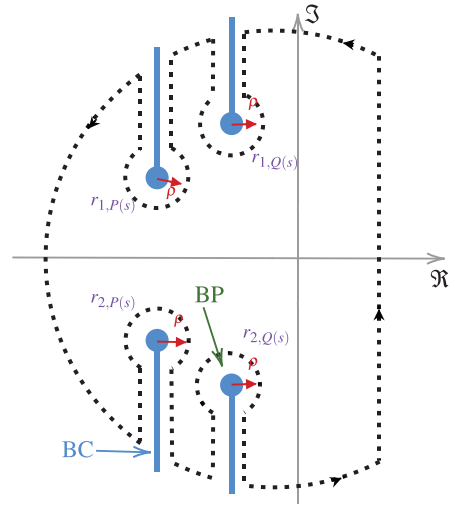

FIGURE 1 Integration contour for system (1)

denotes the set of real numbers (strictly positive, strictly negative) and $\mathbb{N}$ and $\mathbb{Q}$ denote the set of natural and rational numbers respectively. For $\boldsymbol{x}, \boldsymbol{y} \in \mathbb{C}^n$, the inner product is denoted by $\langle \boldsymbol{x}, \boldsymbol{y} \rangle = \boldsymbol{y}^H \boldsymbol{x}$, where $\boldsymbol{y}^H$ is the complex conjugate transpose of $\boldsymbol{y}$. Finally, for $z \in \mathbb{C}$ the modulus of z is designated by $|z|$ and defined as $|z| := \sqrt{\mathfrak{R}\{z\}^2 + \mathfrak{I}\{z\}^2}$.

2 | PRELIMINARY RESULTS AND PROBLEM FORMULATION

In this section, we review some fundamental definitions and preliminary results that will be useful in the remainder of the paper.

Definition 1 (Branch point, branch cut [43, 44]). A branch point (BP) is a point such that the function is discontinuous when going around an arbitrarily small circuit around this point. A branch cut (BC) is the union of two BPs by an arbitrary arc (see Figure 1). This BC connects different sheets of a Riemann surface.

Theorem 1 (from ref. [45]). *A given multi-valued transfer function is stable if and only if it has no poles in $\mathbb{C}_+$ and no BPs in $\mathbb{C}_-$.*

2.1 | Problem formulation

Consider the multi-valued transfer function of the form

$$G(s) = \frac{N(s) + \sqrt{P(s)}}{D(s) + \sqrt{Q(s)}}, \qquad (1)$$

where $N(s) = \sum_{k=0}^{m} b_k s^k$, $D(s) = \sum_{k=0}^{n} a_k s^k$, $a_i, b_i, a_n \neq 0$ are arbitrary real numbers, and $n \geq m$. Besides, $P(s)$ and $Q(s)$ are second order polynomials with positive real coefficients defined
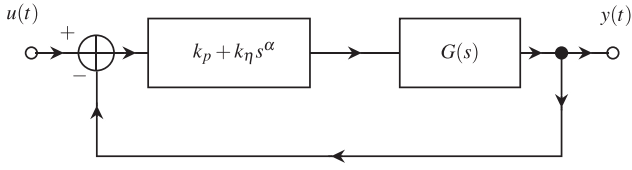
FIGURE 2 Control diagram

as $P(s) = \beta_2 s^2 + \beta_1 s + \beta_0$ and $Q(s) = \gamma_2 s^2 + \gamma_1 s + \gamma_0$, respectively.

In the rest of the paper, we will consider that system (1) is constrained by the following assumptions:

Assumption 1. Polynomials $N(s)$ and $D(s)$ satisfy the following conditions:

(i) $N(s)$ and $D(s)$ are coprime polynomials.
(ii) $|N(i\omega)| > 0, \forall \omega \in \mathbb{R}$.
(iii) if $D(i\omega^*) = 0$, then $|D'(i\omega^*)| > 0$ with $\omega^* \in \mathbb{R}$.

Assumption 2. The functions $P(s)$ and $Q(s)$ satisfy the following condition:

$$\max \left\{ \deg D(s), \frac{1}{2} \deg Q(s) \right\} > \max \left\{ \deg N(s), \frac{1}{2} \deg P(s) \right\}.$$

Assumption 1 permits us to avoid multiple poles on the imaginary axis. It also prevents $D(s)$ and $N(s)$ from having the same roots and allows us to have a strictly proper transfer function even in the case when $\deg Q(s) = \deg P(s) = 0$. On the other hand, Assumption 2 defines rules for the degrees of $P(s), Q(s)$ to obtain a proper transfer function in the case $\deg N(s) = \deg D(s) = 0$.

Given the assumptions above, the problems of our interest are as follows:

Problem 1. Derive conditions on the parameters (k_p, k_η, α) such that the fractional-order controller:

$$C(s) = k_p + k_\eta s^\alpha, \tag{2}$$

BIBO-stabilises the closed-loop plant. Figure 2 describes the closed-loop configuration.

Problem 2. For a fractional controller (2) with given stabilising parameters $\boldsymbol{k}^* = [k_p^*, k_\eta^*, \alpha^*]^T \in \mathbb{R}^3$, determine the maximum positive value d^* and d of the partial fragility analysis and complete fragility analysis, respectively such that the system (1) remains stable:

- Partial fragility analysis: for any k_p and k_η satisfying the following inequality

$$\sqrt{(k_p - k_p^*)^2 + (k_\eta - k_\eta^*)^2} < d^*. \tag{3}$$

- Complete fragility analysis: for any k_p, k_η and α satisfying the following inequality

$$\sqrt{(k_p - k_p^*)^2 + (k_\eta - k_\eta^*)^2 + (\alpha - \alpha^*)^2} < d. \tag{4}$$

3 | MAIN RESULTS

In this section we outline the restrictions of the fractional controller (2) and we give explicit details of the calculation of the stability crossing boundaries of system (1). First, we recall that the closed-loop characteristic function of system (1) is defined as:

$$\Delta(s) := D(s) + \sqrt{Q(s)} + (k_p + k_\eta s^\alpha)(N(s) + \sqrt{P(s)}). \tag{5}$$

Next, the closed-loop transfer function is

$$T(s) = \frac{(N(s) + \sqrt{P(s)})(k_p + k_\eta s^\alpha)}{D(s) + \sqrt{Q(s)} + (N(s) + \sqrt{P(s)})(k_p + k_\eta s^\alpha)} \tag{6}$$

for $\alpha > 0$ and

$$T(s) = \frac{(N(s) + \sqrt{P(s)})(k_p s^\nu + k_\eta)}{(D(s) + \sqrt{Q(s)})s^\nu + (N(s) + \sqrt{P(s)})(k_p s^\nu + k_\eta)}, \tag{7}$$

for $\alpha < 0$ where $-\alpha =: \nu > 0$. Expressions (5), (6) and (7) will be used throughout our analysis.

3.1 | Controller restrictions

It is worth mentioning that an inappropriate selection of the controller degree, that is, an inadequate choice of the parameter α, can cause a loss of causality. Thus, it will be important to impose some restrictions on α. Consequently, throughout this work we will assume that

$$-1 \leq \alpha \leq \overline{\alpha}, \tag{8}$$

where $\overline{\alpha} \in \mathbb{R}_+$ is given as:

$$\overline{\alpha} :=$$

$$\min \left\{ \max \left\{ \deg D(s), \frac{1}{2} \deg Q(s) \right\} \right.$$

$$\left. - \max \left\{ \deg N(s), \frac{1}{2} \deg P(s) \right\}, 1 \right\}.$$

On one hand, the right hand side of inequality (8) is such that the system does not lose causality. On the other hand, the restriction imposed by the left hand side of (8) prevents the system to have multiple poles at the origin.

Apart from the aforementioned restriction on α, consider the following result.

Proposition 1. *Assume that the closed-loop of system (1) is stable. Then,* $|P(s)Q(s)| > 0 \; \forall s \in \mathbb{C}_+$.

Proof. The result follows straightforwardly from Definition 1 and Theorem 1. $\square$

The main consequence of Proposition 1 is that controller (2) is restricted to the class of ISs for which $P(s)$ or $Q(s)$ does not have BPs in $\mathbb{C}_+$. In this regard, since by assumption P and Q fulfil such a property, it follows that control (2) is in possibility to stabilise system (1) in closed-loop, and the restriction imposed by (8) is enough to tackle with Problems 1 and 2 stated above.

3.2 | Stability crossing boundaries

In this section, we focus on finding the stability regions in the (k_p, k_η) parameter-space for different values of α. Hence, the locations of the roots of $\Delta(s)$ will be of our main interest. Therefore, the following result and definitions will be useful:

Definition 2 (Frequency crossing set). The frequency crossing set $\Omega \subset \mathbb{R}$ is the set of all $\omega \in \mathbb{R}$, such that there exists at least a pair (k_p, k_η) for which

$$\Delta(i\omega) = D(i\omega) + \sqrt{Q(i\omega)} + (k_p + k_\eta(i\omega)^\alpha)(N(i\omega)$$
$$+ \sqrt{P(i\omega)}) = 0. \quad (9)$$

Definition 3 (Stability crossing boundaries). The stability crossing boundaries $\mathcal{T}$ is the set of all parameters $(k_p, k_\eta) \in \mathbb{R}^2$ for which there exists at least one $\omega \in \Omega$, such that $\Delta(i\omega) = 0$. Any point $\boldsymbol{k} \in \mathcal{T}$ is known as a crossing point.

3.3 | Stability crossing boundaries characterisation

By following the D-composition method [41], the stability boundaries of system (1) are known to possibly be of three types: complex, real and infinite. In the sequel, we describe the system's stability chart by showing under which conditions for such stability boundaries exist.

3.3.1 | Complex root boundaries

Proposition 2 (Complex root boundaries (CRB), $\alpha \neq 0$). *Let* $\omega \in \mathbb{R}_+$ *and* $\alpha \neq 0$. *Then,* $\omega \in \Omega$ *if and only if* $\boldsymbol{k}(\omega, \alpha) := [k_p(\omega, \alpha), k_\eta(\omega, \alpha)]^T$, *where*

$$k_p(\omega, \alpha) = -\Re\left[\frac{1}{G(i\omega)}\right] + \Im\left[\frac{1}{G(i\omega)}\right] \cot\left(\frac{\alpha\pi}{2}\right), \quad (10)$$

$$k_\eta(\omega, \alpha) = -\Im\left[\frac{1}{G(i\omega)}\right] \omega^{-\alpha} \csc\left(\frac{\alpha\pi}{2}\right). \quad (11)$$

Proof. According to Definition 2, for $s = i\omega$ we look for the pairs $\boldsymbol{k} \in \mathbb{R}^2$ such that,

$$\Delta(i\omega) = 0,$$

$$\Leftrightarrow D(i\omega) + \sqrt{Q(i\omega)} + (k_p + k_\eta(i\omega)^\alpha)(N(i\omega) + \sqrt{P(i\omega)}) = 0,$$

$$\Leftrightarrow \frac{1}{G(i\omega)} + k_p + k_\eta\omega^\alpha\left(\cos\left(\frac{\pi\alpha}{2}\right) + i\sin\left(\frac{\pi\alpha}{2}\right)\right) = 0. \quad (12)$$

Thus, by taking the real and imaginary part of Equation (12) and, solving with respect to k_p and k_η leads to Equations (10) and (11), respectively. $\square$

Proposition 3 (CRB, $\alpha = 0$). *Let* $\omega \in \mathbb{R}_+$ *and* $\alpha = 0$. *Then,* $\omega \in \Omega$ *if and only if* $\boldsymbol{k}(\omega, 0) := [k_p(\omega, 0), k_\eta(\omega, 0)]^T$, *where*

$$k_p(\omega^*, 0) + k_\eta(\omega^*, 0) = -\Re\left[\frac{1}{G(i\omega^*)}\right], \quad \forall \omega^* \in \Omega_{iG}, \quad (13)$$

where Ω_{iG} *is the set defined as*

$$\Omega_{iG} := \left\{\omega \in \mathbb{R}_+ : \Im\left\{\frac{1}{G(i\omega)}\right\} = 0\right\}.$$

Proof. Following similar lines as those presented in the preceding proof, we have:

$$\Delta(i\omega) = 0,$$

$$\Leftrightarrow \frac{1}{G(i\omega)} + k_p + k_\eta\omega^\alpha\left(\cos\left(\frac{\pi\alpha}{2}\right) + i\sin\left(\frac{\pi\alpha}{2}\right)\right) = 0. \quad (14)$$

Now, since $\alpha = 0$, Equation (14) can be rewritten as

$$\Leftrightarrow \frac{1}{G(i\omega)} + k_p + k_\eta = 0. \quad (15)$$

Finally, the proof is concluded by noticing that $1/G(i\omega)$ is a complex number and k_p, k_η must be real, which leads to Equation (13). $\square$

3.3.2 | Real root boundaries

Proposition 4. *The crossing through the origin of the complex plane is given by* $\boldsymbol{k}_0$ *which is defined as*

$$\boldsymbol{k}_0 := \begin{bmatrix} -\frac{a_0 + \sqrt{\alpha_0}}{b_0 + \sqrt{\beta_0}} \\ k_\eta \end{bmatrix}, \quad (16)$$

where $k_\eta \in \mathbb{R}$ for $\alpha > 0$ and

$$\boldsymbol{k}_0 := \begin{bmatrix} k_p \\ 0 \end{bmatrix}, \tag{17}$$

with $k_p \in \mathbb{R}$ for $\alpha < 0$.

Proof. First, let us consider the case $\alpha > 0$. Under this assumption, by taking $s = 0$ in Equation (5), yields:

$$\Delta(0) = 0 \iff \frac{a_0 + \sqrt{\alpha_0}}{b_0 + \sqrt{\beta_0}} + k_p = 0. \tag{18}$$

Thus, clearly $k_p = -\frac{a_0 + \sqrt{\alpha_0}}{b_0 + \sqrt{\beta_0}}$ for every $k_\eta \in \mathbb{R}$, which gives Equation (16). Next, for $\alpha < 0$ the characteristic function (9) can be rewritten as

$$\overline{\Delta}(s) = (D(s) + \sqrt{Q(s)})s^\nu + (k_p s^\nu + k_\eta)(N(s) + \sqrt{P(s)}), \tag{19}$$

where $-\alpha =: \nu > 0$. Hence, by taking $s = 0$, we get:

$$\overline{\Delta}(0) = 0 \iff k_\eta = 0. \tag{20}$$

Therefore, $k_\eta = 0$ for every $k_p \in \mathbb{R}$, which gives Equation (17). $\square$

3.3.3 | Infinite crossing boundaries

Propositions 2 to 4 describe the stability crossing boundaries in the cases when $\Omega \subset \mathbb{R}$. Nevertheless, there exist situations at which a root of Equation (5) can go through one stability region into another by crossing through infinity. Thus, it is of core importance to characterise such infinite crossing boundaries (IRB). Such a characterisation is described by Proposition 5.

Proposition 5. *Consider the characteristic function (5), and let $n_p :=$ deg P and $n_q :=$ deg Q. Then, for $0 < \alpha \le \overline{\alpha}$ an infinite root boundary exists if $\boldsymbol{k}_\infty$ and α satisfy one of the next cases:*

(i) $n \ge \frac{n_q}{2}$

$$\boldsymbol{k}_\infty = \begin{cases} \begin{bmatrix} k_p \\ -\frac{a_n + \chi\sqrt{\gamma_{n_q}}}{b_m} \end{bmatrix}, k_p \in \mathbb{R} & \text{if} \quad \alpha + m = n \text{ and } m > \frac{n_p}{2} \\[2em] \begin{bmatrix} k_p \\ -\frac{a_n + \chi\sqrt{\gamma_{n_q}}}{\sqrt{\beta_{n_p}}} \end{bmatrix}, k_p \in \mathbb{R} & \text{if} \quad \alpha + \frac{n_p}{2} = n \text{ and } m < \frac{n_p}{2} , \\[2em] \begin{bmatrix} k_p \\ -\frac{a_n + \chi\sqrt{\gamma_{n_q}}}{b_m + \sqrt{\beta_{n_p}}} \end{bmatrix}, k_p \in \mathbb{R} & \text{if} \quad \alpha + m = \alpha + \frac{n_p}{2} = n \end{cases} \tag{21}$$

(ii) $\frac{n_q}{2} > n$

$$\boldsymbol{k}_\infty = \begin{bmatrix} k_p \\ -\frac{\sqrt{\gamma_{n_q}}}{\sqrt{\beta_{n_p}}} \end{bmatrix}, k_p \in \mathbb{R}, \tag{22}$$

where $\chi = 0$ if $n > \frac{n_q}{2}$ and $\chi = 1$ if $n = \frac{n_q}{2}$. For $\alpha < 0$ there is no infinite crossing boundary.

Proof. First of all, notice that the infinite crossing boundaries are characterised by the controller values at which Equation (5) loses degree. In this vein, it is easy to see that $\sqrt{Q}$ can be rewritten as follows (for further details, please, see ref. [46]):

$$Q(s) = \sqrt{\gamma_2} s \sqrt{(1 + \frac{z_1}{s})(1 + \frac{z_2}{s})}$$

$$= \sqrt{\gamma_2} s \left(\sum_{j=0}^\infty (-1)^j \binom{1/2}{j} \left(\frac{z_1}{s}\right)^j \sum_{j=0}^\infty (-1)^j \binom{1/2}{j} \left(\frac{z_2}{s}\right)^j \right)$$

$$= \sqrt{\gamma_2} s \left(1 + \mathcal{O}\left(\frac{1}{s}\right) \right),$$

being $-z_1$ and $-z_2$ roots of Q. It is worth mentioning that a similar manipulation can be performed when Q (or P) is a polynomial of degree one. Hence, by expressing $\sqrt{P}$ in the same manner, we can see that both $\sqrt{Q}$ and $\sqrt{P}$ can be written as

$$Q(s) = \sqrt{\gamma_{n_q}} s^{\frac{n_q}{2}} \left(1 + \mathcal{O}\left(\frac{1}{s}\right) \right),$$

$$P(s) = \sqrt{\beta_{n_p}} s^{\frac{n_p}{2}} \left(1 + \mathcal{O}\left(\frac{1}{s}\right) \right). \tag{23}$$

Then, the cases when Equation (5) loses degree can be identified by analysing the closed-loop characteristic equation rewritten as follows

$$\Delta(s) = a_n s^n + \sqrt{\gamma_{n_q}} s^{\frac{n_q}{2}} + k_\eta b_m s^{m+\alpha} + k_\eta \sqrt{\beta_{n_p}} s^{\frac{n_p}{2}+\alpha} + \mathcal{O}(s^{n-1}). \tag{24}$$

Thus, for $\alpha > 0$, (24) leads to the results in Equation (21). Finally, when $\alpha < 0$, from Equation (24) and (19) we see that there is no way to have a loss of degree in the system's characteristic Equation (5). $\square$

3.4 | Crossing directions

The analysis above allows us to determine the values of k_p and k_η at which there exists a solution on the stability boundary. Nonetheless, to determine the stability regions according to the number of unstable roots, we must make a distinction between switches: crossing towards instability and crossing towards stability. For this purpose, the following result will be extremely useful.

Proposition 6. *Consider any $\alpha \neq 0$ satisfying Equation (8). A pair of roots of Equation (5) moves from the LHP to RHP as $\boldsymbol{k}$ crosses the CRB in the increasing direction of k_χ with $\chi \in \{p, \eta\}$, through $\boldsymbol{k}^* = [k_p^*, k_\eta^*]^T$ if:*

$$S_\chi := \Re\left[\frac{s^{\alpha_\chi} \mathcal{E}(i\omega^*)}{\mathcal{D}(i\omega^*)}\right] > 0, \quad (25)$$

where:

$$\mathcal{E}(s) := N(s) + \sqrt{P(s)}, \quad (26)$$

$$\mathcal{D}(i\omega^*) := \left.\frac{\partial D(s)}{\partial s}\right|_{s=i\omega^*} + \left.\frac{\frac{\partial Q(s)}{\partial s}}{2\sqrt{Q(s)}}\right|_{s=i\omega^*}$$

$$+ \left(k_p^* + k_\eta^*(i\omega^*)^\alpha\right)\left.\frac{\partial \mathcal{E}(s)}{\partial s}\right|_{s=i\omega^*}$$

$$+ k_\eta^* \alpha (i\omega^*)^{\alpha-1} \mathcal{E}(i\omega^*), \quad (27)$$

and where the indicative function α_χ is defined as:

$$\alpha_\chi := \begin{cases} 0 & if \quad \chi = p \\ \alpha & if \quad \chi = \eta \end{cases}. \quad (28)$$

The crossing is from the RHP to LHP if the inequality (25) is reversed.

Proof. Let $s \in \mathbb{C}$ be a root of Equation (5), thus the ensuing equality holds:

$$\Delta(s) = 0, \quad (29)$$

$$\Rightarrow D(s) + \sqrt{Q(s)} + \left(k_p + k_\eta s^\alpha\right)\left(N(s) + \sqrt{P(s)}\right) = 0. \quad (30)$$

Now, according to the implicit function theorem (for instance, see ref. [47]), we know that

$$\frac{ds}{dk_p} = -\frac{\frac{\partial \Delta(s)}{\partial k_p}}{\frac{\partial \Delta(s)}{\partial s}}, \qquad \frac{ds}{dk_\eta} = -\frac{\frac{\partial \Delta(s)}{\partial k_\eta}}{\frac{\partial \Delta(s)}{\partial s}} \quad (31)$$

where

$$\frac{\partial \Delta(s)}{\partial s} = \frac{\partial D(s)}{\partial s} + \frac{\frac{\partial Q(s)}{\partial s}}{2\sqrt{Q(s)}} + \left(k_p + k_\eta s^\alpha\right)\frac{\partial \mathcal{E}(s)}{\partial s}$$

$$+ k_\eta \alpha s^{\alpha-1} \mathcal{E}(s),$$

$$\frac{\partial \Delta(s)}{\partial k_p} = N(s) + \sqrt{P(s)} \quad \text{and} \quad \frac{\partial \Delta(s)}{\partial k_\eta} = s^\alpha\left(N(s) + \sqrt{P(s)}\right).$$

Now, by taking $s = i\omega^*$ we get

$$S_p := \Re\left[\left.\frac{ds}{dk_p}\right|_{s=i\omega^*, \boldsymbol{k}=\boldsymbol{k}^*}\right] \quad \text{and} \quad S_\eta := \Re\left[\left.\frac{ds}{dk_\eta}\right|_{s=i\omega^*, \boldsymbol{k}=\boldsymbol{k}^*}\right].$$

Therefore, as $\boldsymbol{k}$ crosses in any direction from left to right of $\mathcal{T}$, one root of Equation (5) crosses from the LHP to RHP of the complex plane through $i\omega$ if $S_p > 0$ ($S_\eta > 0$), implying that $k_p > k_p^*$ ($k_\eta > k_\eta^*$). Furthermore, the crossing is from the RHP to the LHP if $S_p < 0$ ($S_\eta < 0$), that is, $k_p < k_p^*$ ($k_\eta < k_\eta^*$), as stated in Proposition 6. □

3.5 | Fragility analysis

As mention in the Introduction, we know that every controller implementation is subject to the imprecision due to different factors: finite word length or round-off errors in numerical computations, for instance. Hence, it is important to find out a way to effectively quantify the maximum controller parameters deviation of a given stabilising controller $\boldsymbol{k}^* = (k_p^*, k_\eta^*, \alpha^*)$. This maximum parameter deviation is called fragility. In this section, we will consider the fragility problem in the partial parameter-space (k_p, k_η) for a fixed α and in the complete parameter-space (k_p, k_η, α), i.e. in two and three dimensions, respectively.

3.5.1 | Partial parameter-space analysis

For a fixed α, in the parameter plane (k_p, k_η) the maximum deviation d^* of a given stabilising controller $\boldsymbol{k}^*$ can be studied by the next inequality:

$$\sqrt{(k_p - k_p^*)^2 + (k_\eta - k_\eta^*)^2} < d^*. \quad (32)$$

For a fixed $\boldsymbol{k}^* = (k_p^*, k_\eta^*)^T \in \mathbb{R}^2$ and $\boldsymbol{k}(\omega, \alpha) := (k_p(\omega, \alpha), k_\eta(\omega, \alpha))^T$, let us introduce $\xi : \mathbb{R}_+ \times \mathbb{R} \to \mathbb{R}_+$ as:

$$\xi(\omega, \alpha) := \sqrt{(k_p(\omega, \alpha) - k_p^*)^2 + (k_\eta(\omega, \alpha) - k_\eta^*)^2}. \quad (33)$$

We have the following result:

Proposition 7. *Let $\boldsymbol{k}^* = (k_p^*, k_\eta^*)^T$ be a fixed stabilising controller. Then, for α satisfying $0 < \alpha < \overline{\alpha}$, the maximum parameter deviation d^* of $\boldsymbol{k}^*$ without losing stability is given by:*

$$d^* := \min\left\{d_\omega^*, d_0^*, d_\infty^*\right\}, \quad (34)$$

where d_ω^*, d_0^* and d_∞^* are given by:

$$d_\omega^* := \min_{\omega \in \Omega_{f_{\boldsymbol{k}^*}}}\{\xi(\omega, \alpha)\}, \quad d_0^* := \frac{a_0 + \sqrt{\alpha_0}}{b_0 + \sqrt{\beta_0}} + k_p^*, \quad d_\infty^* := \ell_\alpha + k_\eta^*. \quad (35)$$

Here $\Omega_{f_{\boldsymbol{k}^*}}$ *denotes the set of all roots of* $f_{\boldsymbol{k}^*}(\omega, \alpha)$ *defined as:*

$$f_{\boldsymbol{k}^*}(\omega, \alpha) := \left\langle \boldsymbol{k}(\omega, \alpha) - \boldsymbol{k}^*, \frac{d\boldsymbol{k}(\omega, \alpha)}{d\omega} \right\rangle, \qquad (36)$$

where ℓ_α *in Equation (35) is defined as*

(i) $n \geq \frac{n_q}{2}$

$$\ell_\alpha := \begin{cases} \frac{a_n + \chi\sqrt{\gamma_{n_q}}}{b_m} & if \quad \alpha + m = n \text{ and } m > \frac{n_p}{2} \\ \frac{a_n + \chi\sqrt{\gamma_{n_q}}}{\sqrt{\beta_{n_p}}} & if \quad \alpha + \frac{n_p}{2} = n \text{ and } m < \frac{n_p}{2}, \\ \frac{a_n + \chi\sqrt{\gamma_{n_q}}}{b_m + \sqrt{\beta_{n_p}}} & if \quad \alpha + m = \alpha + \frac{n_p}{2} = n \end{cases} \qquad (37)$$

(ii) $n < \frac{n_q}{2}$

$$\ell_\alpha := \frac{\sqrt{\gamma_{n_q}}}{\sqrt{\beta_{n_p}}}. \qquad (38)$$

Here $\chi = 0$ *if* $n > \frac{n_q}{2}$ *and* $\chi = 1$ *if* $n = \frac{n_q}{2}$. *On the other hand, for* $\alpha < 0$, *the maximum parameter deviation* d^* *is*

$$d^* = \min\{d^*_\omega, d^*_0\}, \qquad (39)$$

where d^*_ω *is obtained from Equation (35) and*

$$d^*_0 := k^*_\eta. \qquad (40)$$

Proof. Since by hypothesis $\boldsymbol{k}^*$ belongs to a stability region, it is sufficient to show that the minimum distance d to the stability boundaries (CRB, real root boundaries [RRB], IRB) is given by Equations (34) and (39) for $\alpha > 0$ and $\alpha < 0$, respectively. To this end, let us consider first the distance to the CRB which exists for any value of α. According to Proposition 2, in this situation we must have $\omega \in \Omega \setminus \{0\}$. Next, we will identify the frequencies at which the vectors $\frac{d}{d\omega}\boldsymbol{k}(\omega, \alpha)$ and $\boldsymbol{k}(\omega, \alpha) - \boldsymbol{k}^*$ are orthogonal, since at such frequencies occur the minimum distance. Therefore, d_ω in Equation (35) will compute such a value. Next, for the distance to the RRB boundary which is different depending on the value of α. For $\alpha > 0$ we have to consider the case described in Proposition 4. Now, substituting Equation (16) into Equation (33) leads to:

$$\xi(0, \alpha) = \sqrt{\left(\frac{a_0 + \sqrt{\gamma_0}}{b_0 + \sqrt{\beta_0}} + k^*_p\right)^2 + (k_\eta - k^*_\eta)^2}. \qquad (41)$$

By solving $\frac{d\xi^2(0, \alpha)}{dk_\eta} = 0$, we find the value at which $\xi(0, \alpha)$ reaches its minimum. Then, by substituting this value in

Equation (33) we find d_0 given by Equation (35). For $\alpha < 0$ we follow the same steps to obtain the distance d_0 in Equation (35).

Finally, we need to compute the distance to the IRB boundary which only exists for $\alpha > 0$ according to Proposition 5. To such an end, let us denote such a distance by ξ_∞. Hence, substituting each of the cases shown in Equations (21) and (22) of Proposition 5 into Equation (33) leads to

$$\xi_\infty = \sqrt{(k_p - k^*_p)^2 + (\ell + k^*_\eta)^2}, \qquad (42)$$

where ℓ is defined in Equations (37) and (38). Thus, performing similar analysis to those used in the computation of the distance to the RRB, we find that the minimum distance is given by d_∞ in Equation (35). Finally, Equation (35) follows by taking the minimum distance to all boundaries for $\alpha > 0$ and by (39) for $\alpha < 0$. □

3.5.2 | Complete parameter-space analysis

Proposition 7 allows us to measure the fragility of a controller by considering a fixed fractional-order α. This assumes that α does not have any kind of imprecision problems as the controller gains k_p or k_η do. However, by considering the fact that fractional-order operators must always be discretized for its implementation (the methods of Oustaloup, Matsuda, AbdelAty or El-Khazali are the usual discretization techniques for such a purpose, see, for instance ref. [48]), then, we can conclude that α is the controller's parameter with the highest imprecision and, as a consequence, it will be crucial to measure its fragility.

In view of the above discussion, Algorithm 1 describes a procedure that enables us to compute the controller's fragility in the parameter-space (k_p, k_η, α). The solution give us the maximum deviation d of a stabilising controller $\boldsymbol{k}^* = (k^*_p, k^*_\eta, \alpha^*)$. The value d is the radius of a sphere which is fully contained in the stability region.

4 | NUMERICAL EXAMPLES

In this section, we discuss some special cases of ISs to illustrate the utility of the results obtained in the previous sections. Firstly, every example shows a stability region analysis plot for a fixed α in the parameter-plane (k_p, k_η) where we also show the behaviour of S_χ according to Proposition 6 while depicting the growing direction of curves when increasing the value of ω on the plots. To distinguish between each of the stability crossing boundaries we use the colours: blue for the CRB, red for the RRB and yellow for the IRB. In addition, to emphasise the stable region in the (k_p, k_η)-parameter plane we shade the region in grey colour. Secondly, we give plots of the stability region in the parameter-space (k_p, k_η, α) for $\alpha > 0$ and for $\alpha < 0$. Some of the examples show the fragility analysis considering Proposition 7 or Algorithm 19 for specific arbitrarily chosen gains. Finally, every example shows a plot with the

ALGORITHM 1 Complete Fragility Analysis

```
/* For a given α* ∈ ℝ\0, let (kₚ*,kη*,α*) be a
   stabilizing triplet for system (1). */
```

Data: Consider the initial data: $(k_p^*, k_\eta^*, \alpha^*)$.

Result: The complete fragility d of the triplet $(k_p^*, k_\eta^*, \alpha^*)$.

1 Let $\widehat{d_\infty} := \begin{cases} d_\infty^* & \text{if } \alpha > 0 \\ +\infty & \text{if } \alpha < 0 \end{cases}$, $j := 0$, set

$d := \min\left\{d_\omega^*, d_0^*, \widehat{d_\infty}, |\alpha^*|\right\}$ and let (θ_j) be a finite strictly increasing sequence in $\left[-\frac{\pi}{2}, \frac{\pi}{2}\right]$, such that $\theta_0 := -\frac{\pi}{2}$ and $\theta_N := \frac{\pi}{2}$.

2 **while** $\theta_j \leq \frac{\pi}{2}$ **do**

3   **if** $\alpha^* > 0$ **then**

4   set $\alpha_{\theta_j} := \alpha^* + d\sin(\theta_j)$;

5   solve $f_{k^*}(\omega, \alpha_{\theta_j}) = 0$ and denote by $\Omega_{f_{\theta_j}}$ the set of solutions;

6   compute

$d_{\theta_j}^* := \min_{\omega_r \in \Omega_{f_{\theta_j}}} \left\{\xi\left(\omega_r, \alpha_{\theta_j}\right), \ell_{\alpha_{\theta_j}} + k_\eta^*, |\alpha^*|\right\}$;

7   **if** $d_{\theta_j}^* < d\cos(\theta_j)$ **then**

8        $d := \frac{d_{\theta_j}^*}{\cos(\theta_j)}$;

9   **end**

10   **else**

11   set $\alpha_{\theta_j} := \alpha^* + d\sin(\theta_j)$;

12   solve $f_{k^*}(\omega, \alpha_{\theta_j}) = 0$ and denote by $\Omega_{f_{\theta_j}}$ the set of solutions;

13   compute $d_{\theta_j}^* := \min_{\omega_r \in \Omega_{f_{\theta_j}}} \left\{\xi\left(\omega_r, \alpha_{\theta_j}\right), |\alpha^*|\right\}$;

14   **if** $d_{\theta_j}^* < d\cos(\theta_j)$ **then**

15        $d := \frac{d_{\theta_j}^*}{\cos(\theta_j)}$;

16   **end**

17   **end**

18    $j = j + 1$;

19 **end**

(a) The (k_p, k_η) stability region analysis for $\alpha = 0.6$ (Propositions 2, 4 and 5) and the sign crossing behavior (Proposition 6).
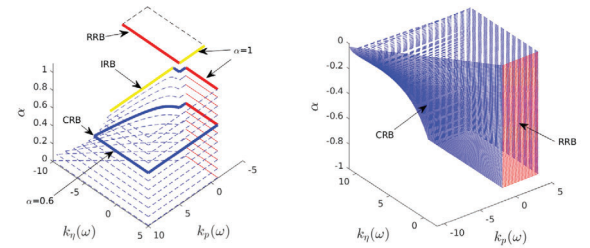
(b) The (k_p, k_η, α) stability region for $\alpha > 0$. (c) The (k_p, k_η, α) stability region for $\alpha < 0$.
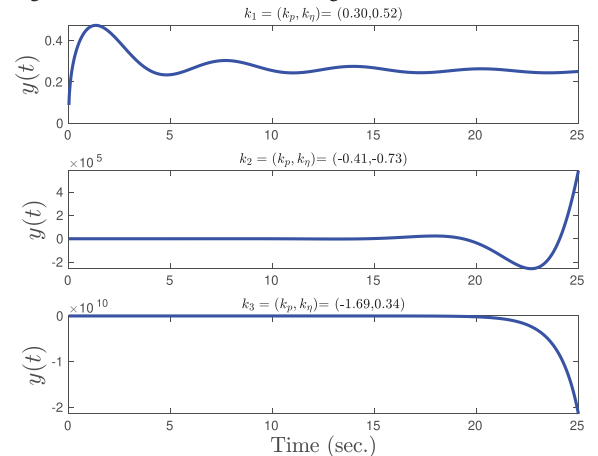
(d) Time step response of the closed-loop of system (43) with distinct controller gains. Controller gain locations are illustrated in Fig. 3(a).

FIGURE 3 Stability region analysis for system (43)

closed-loop time responses considering the gains depicted in a given parameter plane k_p, k_η for a fixed α. For all the closed-loop system responses presented in this section, we use the numerical inverse Laplace transform method presented in ref. [49].
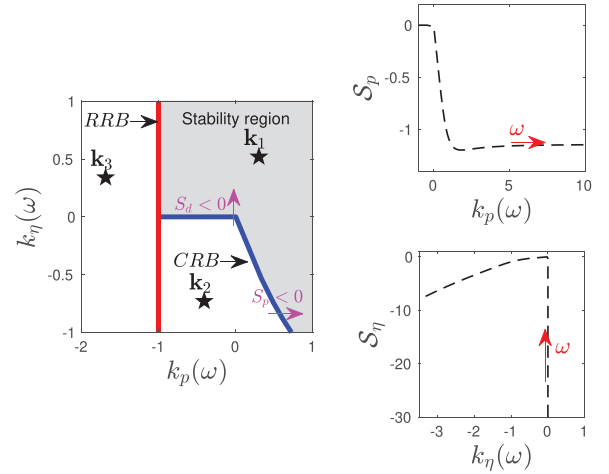
4.1 | Bessel system

As the first example, consider the Laplace transform of the Bessel function of order zero described as

$$H(s) = \frac{1}{\sqrt{s^2 + 1}}. \tag{43}$$

Note that the Bessel function of zero-order is known as the solution of a second-order differential equation given by $x(y'' + y) + y' = 0$. With a fractional controller, the closed-loop system characteristic equation for Equation (43) becomes

$$\Delta_{\text{bessel}}(s) = \sqrt{s^2 + 1} + k_p + k_\eta s^\alpha. \tag{44}$$

From Equation (8) we have $-1 \leq \alpha \leq 1$. For a fixed value of $\alpha = 0.6$ Propositions 4, 2 and 5 allow us to determine the

crossing root boundaries as shown in Figure 3a. Moreover, Figure 3a shows the use of Proposition 6 by plotting Equation (25) in the k_p and k_η direction. For every $\omega \neq 0$, Equation (25) gives us a point of departure to determine the stability region shown in the shaded region of Figure 3a. By applying our methodology repetitively for values of $\alpha > 0$ we show the stability space in Figure 3b. We emphasise in thick colours the slice corresponding to $\alpha = 0.6$ which is also depicted in Figure 3a and the slice corresponding to $\alpha = 1$ which is the only
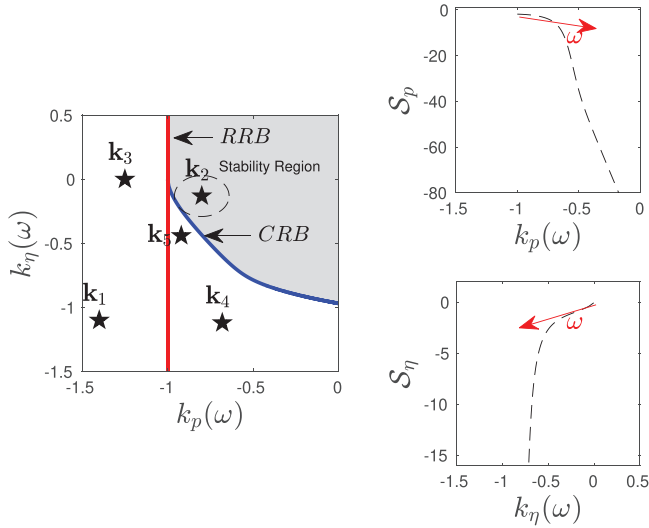
(a) The (k_p, k_η) stability region analysis given $\alpha = 0.4$ (Propositions 2, 4 and 5) and the sign crossing behavior (Proposition 6). Besides, the fragility of k_2 is depicted.
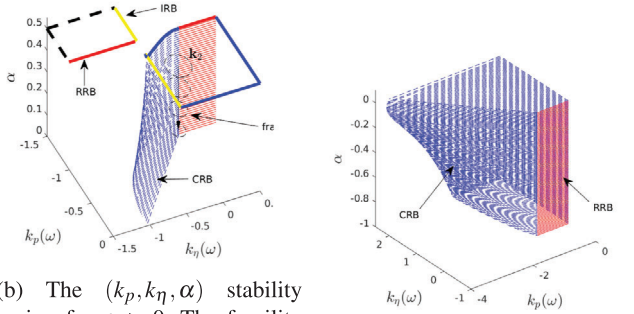
(b) The (k_p, k_η, α) stability region for $\alpha > 0$. The fragility for k_2 is shown for different values of α.

(c) The (k_p, k_η, α) stability region for $\alpha < 0$.
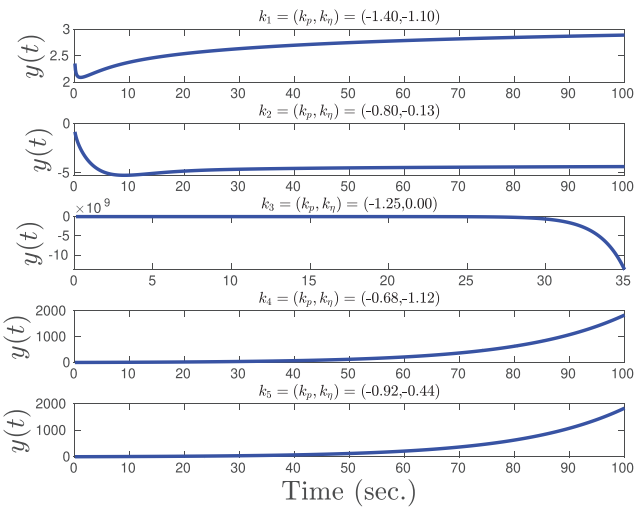
(d) Time impulse response of the closed-loop of system (45) with distinct controller gains. Controller gain locations are illustrated in Fig. 4(a).

FIGURE 4   Stability region analysis for system (45)

TABLE 1   Fragility analysis of system (45)

Fragility analysis k_2				
α	d_0	d_ω	ω	d^*
0.4	0.2	0.1562	0.0874	0.1562
0.3	0.2	0.1350	0.0859	0.1350
0.2	0.2	0.1122	0.0700	0.1122
0.1	0.2	0.0867	0.0418	0.0867

case where an IRB exists. Figure 3c shows the stability space for $\alpha < 0$.

Finally, by choosing any (k_p, k_η) parameters inside each of the three regions enclosed by the stability crossing boundaries in Figure 3a, we show the step responses shown in Figure 3d.

4.2 | First order IS

Consider the IS given by

$$H(s) = \frac{\sqrt{3s + 1}}{s + \sqrt{2s + 1}}. \tag{45}$$

To implement a fractional-order controller (2) to this system, we first develop the stability crossing boundaries depicted in Figure 4a for a fixed $\alpha = 0.4$ by means of Propositions 5 and 4.

In this example, we make use of Proposition 7 to determine the maximum parameter deviation for an arbitrarily chosen stabilising controller k_2 inside the stability region shown in Figure 4a. The values and fragility of k_2 for different fixed values of α are shown in Table 1. Furthermore, we plot the stability space in Figure 4b for $\alpha > 0$ and Figure 4c for $\alpha < 0$. Also, in Figure 4b, we plot the fragility of k_2 for several fixed values of α. From Figure 4b, we can see that there is a IRB only when $\alpha = 0.5$ according to Proposition 5.

Finally, to prove the behaviour of the closed-loop system, we illustrate the step response in Figure 4d for various arbitrarily chosen controller gains for $\alpha = 0.4$.

4.3 | Infinite tree of springs and dampers

Consider the following IS which was proposed to describe the total transfer function of the infinite tree of springs and dampers shown in Figure 5 (for further details, see ref. [5, 7]).

$$G_x(s) = \frac{\varrho + \sigma s + \sqrt{(\varrho + \sigma s)^2 + \varsigma s}}{ms^2 + \varrho + \sigma s + \sqrt{(\varrho + \sigma s)^2 + \varsigma s}}, \tag{46}$$

where $\varrho = (p-1)k, \sigma = (q-1)b, \varsigma = 4(p+q-1)kb$ and $m = 2m_{\text{last}}$. Here, $p \geq 1$ is the number of springs with spring constant k and $q \geq 1$ is the number of dampers with damping constant b and m_{last} is the mass of the last element in the infinite tree [5].
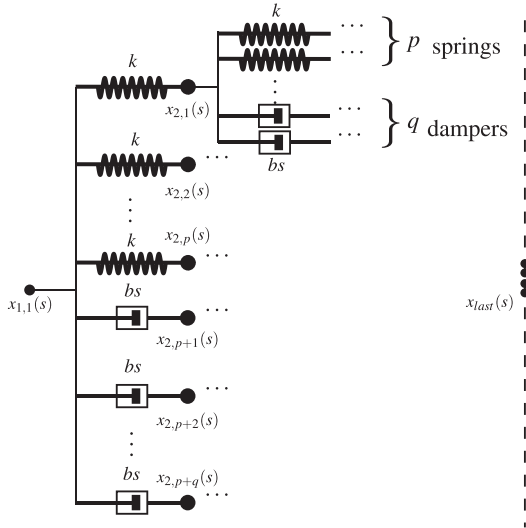
FIGURE 5   Infinite tree of springs and dampers

Considering the case when the system parameters are $p = 2$, $q = 2$, $k = 0.2$, $b = 0.4$ and $m_{last} = 1$, we make the following transfer function:

$$G_x^*(s) = \frac{0.2 + 0.4s + \sqrt{(0.4s + 0.2)^2 + 0.96s}}{2s^2 + 0.2 + 0.4s + \sqrt{(0.4s + 0.2)^2 + 0.96s}}. \quad (47)$$

The stability analysis for system (46) subject to a fractional controller (2) is depicted in Figure 6. A special case for $\alpha = 0.4$ is shown in Figure 6b. The stability region is similarly found by means of Propositions 2, 4 and 5. Again, the stability region is detected by studying the sign of S_χ as described in Proposition 6. We also depict the stability space for different values of (k_p, k_η, α) in Figure 6a and c. We can see from Figure 6a that there is also a IRB when $\alpha = 1$ according to Proposition 5. Furthermore, we use Algorithm 19 to find the fragility in the parameter-space (k_p, k_η, α) of controller $\mathbf{k}_1 = (k_p^*, k_\eta^*, \alpha^*) = (0.528, -0.87, 0.4)$. The fragility sphere is depicted in Figure 6a. Finally, to show the behaviour of the closed-loop system, we illustrate the step response in Figure 6d for various arbitrarily chosen controller gains shown in Figure 6b.

4.4 | Higher order IS

Consider the third order IS given by

$$H(s) = \frac{s^2 + 2s + 1 + \sqrt{2s + 3}}{s^3 + 3s^2 + 4s - 2 + \sqrt{s + 1}}. \quad (48)$$

By analysing the closed-loop characteristic polynomial of system (48) subject to the fractional-order controller, we are able to find its stability region in Figure 7. Such stability chart shows a more complicated structure but our Propositions 2, 4 and 5 can still be applied. In Figure 7a, we consider the case when $\alpha = 0.8$. As
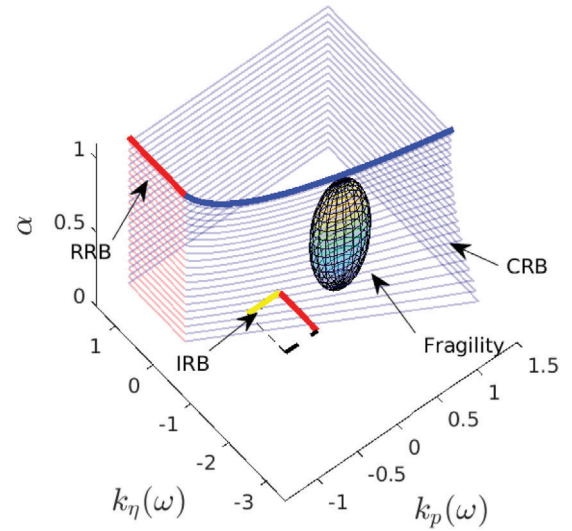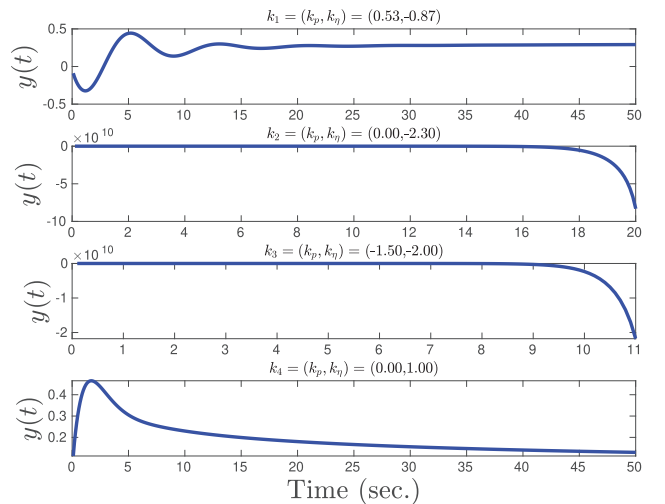

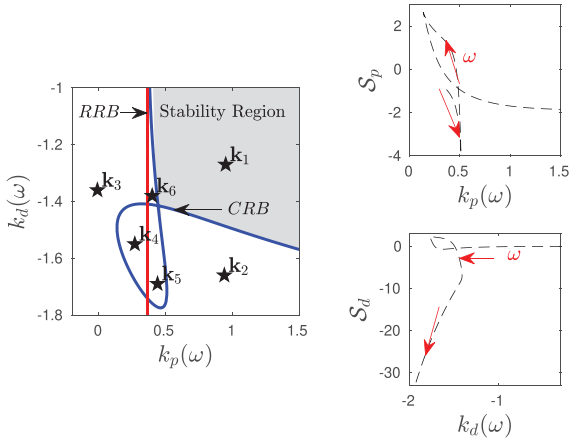(a) The (k_p, k_η, α) stability region for $\alpha > 0$.
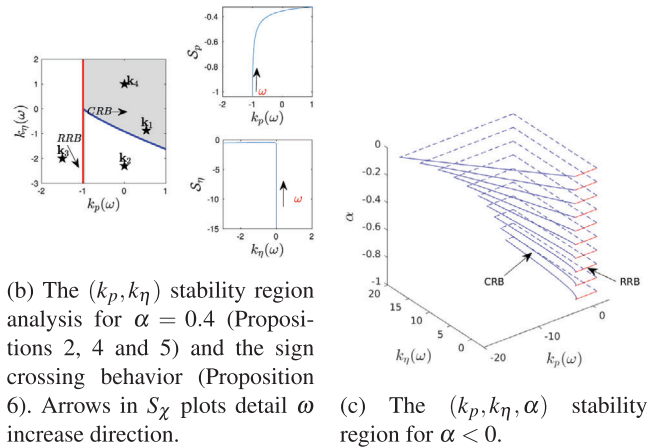
(b) The (k_p, k_η) stability region analysis for $\alpha = 0.4$ (Propositions 2, 4 and 5) and the sign crossing behavior (Proposition 6). Arrows in S_χ plots detail ω increase direction.

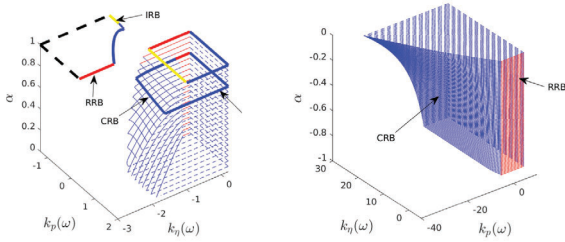(c) The (k_p, k_η, α) stability region for $\alpha < 0$.

(d) Time impulse response of the closed-loop of system (46) with distinct controller gains. Controller gain locations are illustrated in Fig. 6(b).
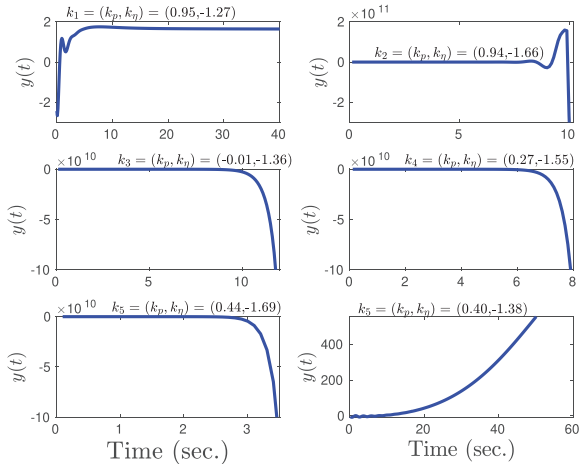
FIGURE 6   Stability region analysis for system (46)

(a) The (k_p, k_η) stability region analysis for $\alpha = 0.8$ (Propositions 2, 4 and 5) and the sign crossing behaviour (Proposition 6).

(b) The (k_p, k_η, α) stability region for $\alpha > 0$.

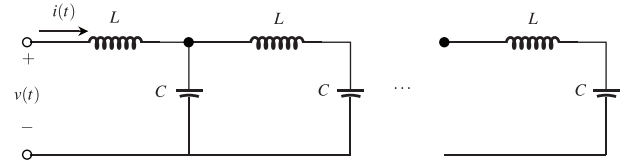(c) The (k_p, k_η, α) stability region for $\alpha < 0$.

(d) Time step response of the closed-loop system with distinct controller gains. Controller gain locations are illustrated in Fig. 7(a).
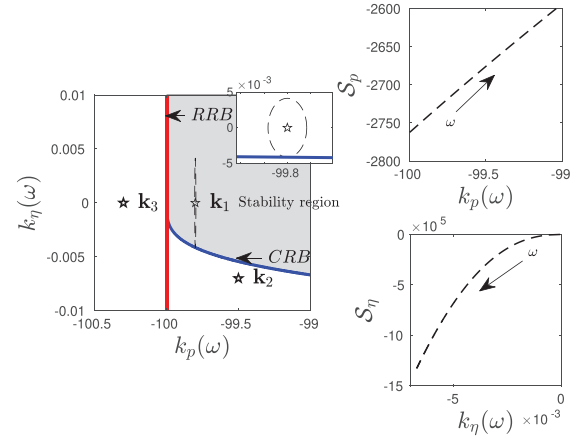
FIGURE 7   Stability region analysis for system (48)

in the previous examples, we have the S_χ plots in Figure 7a with the increasing direction of ω in order to study the roots crossing behaviour of the closed-loop characteristic equation.

Plots for various $\alpha > 0$ and $\alpha < 0$ are depicted in Figure 7b and c, respectively. From Figure 7b, we can see that we have eliminated the loops that the CRB creates when ω goes from 0 to infinity for certain values of α to only depict the stable regions which correspond to the enclosed areas. Finally, for arbitrarily chosen controller gains displayed in Figure 7a, the step response of the closed-loop system is illustrated in Figure 7d.
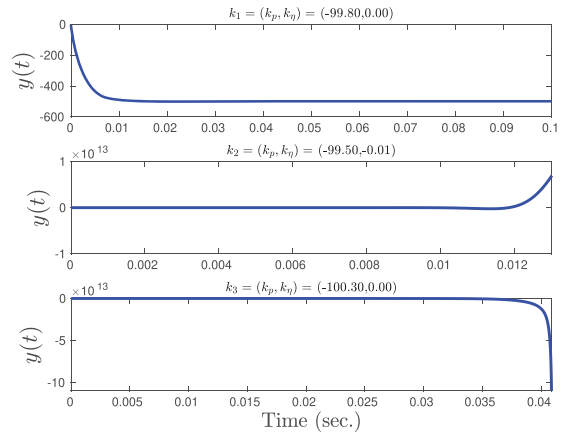

(a) Infinite LC ladder electrical circuit.

(b) The (k_p, k_η) stability region analysis for $\alpha = 0.7$ (Propositions 2, 4 and 5) and the sign crossing behaviour (Proposition 6).
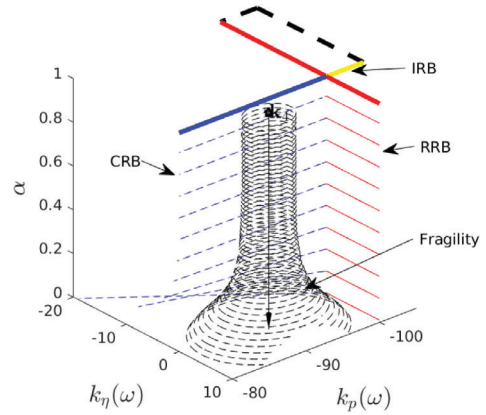
(c) The (k_p, k_η, α) stability region and fragility of $k_4 = (-90, 3)$ with $\alpha > 0$.

(d) System (49) response with various controller gains taken from Fig. 8(b).

FIGURE 8   Stability region analysis for system (49)

4.5 | Infinite LC ladder network

The last example is the infinite LC ladder network (see Figure 8a) whose admittance, under certain conditions, is given by [9, 11]

$$G(s) = \cfrac{1}{z_0 \left(\dfrac{s}{2\omega_0} \pm \sqrt{1 + \left(\dfrac{s}{2\omega_0} \right)^2} \right)}, \qquad (49)$$

with $z_0 = \sqrt{\dfrac{L}{C}}$ and $\omega_0 = \dfrac{1}{\sqrt{LC}}$. The closed-loop characteristic equation is given by

$$\Delta(s) = 2k_\eta \omega_0 s^\alpha + 2k_p \omega_0 + z_0 \left(\omega_0 \sqrt{\dfrac{s^2}{\omega_0^2} + 4} + s \right). \qquad (50)$$

By selecting $C = .1\mu$F and $L = 1m$H we perform the stability analysis as in our previous examples. The results are summarised in Figure 8. Here we also analyse the fragility for two controller values k_1 and k_2. The k_1 fragility is shown in Figure 8b while k_2 fragility is shown in Figure 8c for several values of $\alpha > 0$. Finally, in this example we also show the system response in Figure 8d when using the controller gains k_1, k_2 and k_3 shown in Figure 8b.

5 | CONCLUDING REMARKS

Throughout this work, we have presented a geometrical methodology for finding the closed-loop stability space for a type of ISs controlled by fractional-order controllers. Since ISs can be found when modelling certain large-scale networks, it is of fundamental importance to propose controller schemes to deal with such systems. In this regard, our results represent, to the best of the author's knowledge, the first contribution in this direction. The detailed theoretical results were accompanied by several numerical examples related to real applications that illustrate their utility. Besides, the controller gains from the stability space guarantee a BIBO stability. Future studies may include the extension of our analysis to address the full fractional-order $PI^\lambda D^\mu$ controller, other kinds of multi-valued complex functions as well as an analytical method to design the system's transient response.

ORCID
Adrian-Josue Guel-Cortez https://orcid.org/0000-0002-9325-9956

REFERENCES

1. Sen, M., et al.: Implicit and fractional-derivative operators in infinite networks of integer-order components. Chaos Solitons Fractals 114, 186–192 (2018)
2. Mayes, J., Sen, M.: Approximation of potential-driven flow dynamics in large-scale self-similar tree networks. Proc. R. Soc. Lond. A, Math. Phys. Eng. Sci. 467(2134), 2810–2824 (2011)
3. Montseny, G.: Diffusive representation of pseudo-differential time-operators. ESAIM: Proc 5, 159–175 (1998)
4. Casenave, C., Montseny, G.: Introduction to diffusive representation. IFAC Proc. Vol. 43(21), 370–377 (2010)
5. Goodwine, B.: Approximations for implicitly-defined dynamics of networks of simple mechanical components. Proc. 2018 26th Mediterranean Conference on Control and Automation (MED), Zadar, Croatia, pp. 454–459 (2018)
6. Leyden, K., Goodwine, B.: Using fractional-order differential equations for health monitoring of a system of cooperating robots. Proc. 2016 IEEE Int. Conf. on Robotics and Automation (ICRA), Stockholm, pp. 366–371 (2016)
7. Guel-Cortez, A.J., Sen, M., Goodwine, B.: Closed form time response of an infinite tree of mechanical components described by an irrational transfer function. Proc. 2019 American Control Conference (ACC), Philadelphia, PA, USA, pp. 5828–5833 (2019)
8. Feynman, R.P., Leighton, R.B., Sands, M.: The Feynman Lectures on Physics: Volume II, Pearson, New York (2006)
9. Klimo, P.: On the impedance of infinite LC ladder networks. Eur. J. Phys. 38(1), 015805 (2016)
10. Leyden, K., Sen, M., Goodwine, B.: Large and infinite mass-spring-damper networks. ASME, J. Dyn. Syst. Meas. Control 141(6), 061005 (2019)
11. Kelly, J.F., MacGough, R.J.: Fractal ladder model and power law wave equations. J. Acoust. Soc. Am. 126(4), 2072–2081 (2009)
12. Curtain, R.F., Zwart, H.: An Introduction to Infinite-Dimensional Linear Systems Theory. Springer-Verlag, New York (2012)
13. Hernández, D., Núñez-López, M., Velasco-Hernández, J.X.: Telegraphic double porosity models for head transient behavior in naturally fractured aquifers. Water Resour. Res. 49(7), 4399–4408 (2013)
14. Wu, Y., et al.: A triple-continuum pressure-transient model for a naturally fractured vuggy reservoir. Lawrence Berkeley National Laboratory 210082898 (2007)
15. Zhang, J., Yang, G.: Prescribed performance fault-tolerant control of uncertain nonlinear systems with unknown control directions. IEEE Trans. Autom. Control 62(12), 6529–6535 (2017)
16. Zhang, J., Yang, G.: Low-complexity tracking control of strict-feedback systems with unknown control directions. IEEE Trans. Autom. Control 64(12), 5175–5182 (2019)
17. Zhang, J., Yang, G.: Fault-tolerant output-constrained control of unknown euler–lagrange systems with prescribed tracking accuracy. Automatica 111, 108606 (2020)
18. Fliess, M., Join, C.: Model-free control. Int. J. Control 86(12), 2228–2252 (2013)
19. Bieker, K., et al.: Deep model predictive flow control with limited sensor data and online learning. Theor. Comput. Fluid Dyn. 34, 577–591 (2020)
20. Shah, P., Agashe, S.: Review of fractional PID controller. Mechatronics 38, 29–41 (2016)
21. Wang, C., Zhao, Y.: Performance analysis and control of fractional-order positive systems. IET Control Theory Appl. 13(7), 928–934 (2019)
22. Guel-Cortez, A.J., et al.: Geometrical design of fractional $PD\mu$ controllers for linear time-invariant fractional-order systems with time delay. Proc. Inst. Mech. Eng. I, J. Syst. Control Eng. 233(7), 815–829 (2019)
23. Yu, Z., et al.: Distributed adaptive fractional-order fault-tolerant cooperative control of networked unmanned aerial vehicles via fuzzy neural networks. IET Control Theory Appl. 13(17), 2917–2929 (2019)
24. Caponetto, R.: Fractional Order Systems: Modeling and Control Applications. World Scientific, Singapore (2010)
25. Monje, C.A., et al.: Fractional-order Systems and Controls: Fundamentals and Applications. Springer, London (2010)

26. Tavazoei, M.S.: From traditional to fractional PI control: A key for generalization. IEEE Ind. Electron. Mag. 6(3), 41–51 (2012)

27. Valério, D., da Costa, J.S.: An Introduction to Fractional Control. Institution of Engineering and Technology, London (2013)

28. Podlubny, I.: Fractional-order systems and $PI^\lambda D^\mu$-controllers. IEEE Trans. Autom. Control 44(1), 208–214 (1999)

29. Petráš˘, I., (Ed.). Hanbook of Fractional Calculus with Applications. Volume 6 Applications in Control. De Gruyter, Berlin (2019)

30. Ghorbani, M., Tavakoli-Kakhki, M., Estarami, A.A.: Robust FOPID stabilization of retarded type fractional order plants with interval uncertainties and interval time delay. J. Franklin Inst. 356(16), 9302–9329 (2019)

31. Gao, Z.: Analytical method on stabilisation of fractional-order plants with interval uncertainties using fractional-order $PI^\lambda D^\mu$ controllers. Int. J. Syst. Sci. 50(5), 935–953 (2019)

32. Birs, I., et al.: A survey of recent advances in fractional order control for time delay systems. IEEE Access 7, 30951–30965 (2019)

33. Liu, L., et al.: General robustness analysis and robust fractional-order PD controller design for fractional-order plants. IET Control Theory Appl. 12(12), 1730–1736 (2018)

34. Badri, V., Tavazoei, M.S.: Stability analysis of fractional order time-delay systems: constructing new Lyapunov functions from those of integer order counterparts. IET Control Theory Appl. 13(15), 2476–2481 (2019)

35. Zhang, X., Chen, Y.: Admissibility and robust stabilization of continuous linear singular fractional order systems with the fractional order α: The $0 < \alpha < 1$ case. ISA Trans. 82, 42–50 (2018)

36. Guel-Cortez, A.J., et al.: Fractional-$\boldsymbol{PD^\mu}$ controllers for irrational systems. Proc. 2019 6th Int. Conf. on Control, Decision and Information Technologies, Paris, pp. 13–18 (2019)

37. Méndez-Barrios, C., et al.: On the fragility of PI controllers for time-delay SISO systems. Proc. 2008 16th Mediterranean Conference on Control and Automation, IEEE, Piscataway, NJ, pp. 529–534 (2008)

38. Keel, L.H., Bhattacharyya, S.P.: Robust, fragile, or optimal? IEEE Trans. Autom. Control 42(8), 1098–1105 (1997)

39. Alfaro, V.M.: PID controllers' fragility. ISA Trans. 46(4), 555–559 (2007)

40. Ho, M.T.: Non-fragile PID controller design. Proc. Proceedings of the 39th IEEE Conference on Decision and Control (Cat. No. 00CH37187), Sydney, pp. 4903–4908 (2000)

41. Gryazina, E.N., Polyak, B.T., Tremba, A.A.: D-decomposition technique state-of-the-art. Autom. Remote Control 69(12), 1991–2026 (2008)

42. Gryazina, E.N.: The D-decomposition theory. Autom. Remote Control 65(12), 1872–1884 (2004)

43. Cohen, H.: Complex Analysis with Applications in Science and Engineering. Springer, Boston, MA (2007)

44. Needham, T.: Visual Complex Analysis. Clarendon Press, Oxford (1997)

45. Merrikh-Bayat, F., Karimi-Ghartemani, M.: On the essential instabilities caused by fractional-order transfer functions. Math. Prob. Eng. 2008, 1–13 (2008)

46. Goss, D.: The ongoing binomial revolution. In: Bars, F., Longhi, I., Trihan, F., (Eds.): Arithmetic Geometry Over Global Function Fields. Birkhäuser, Basel, CRM Barcelona, pp. 183–193 (2014)

47. LePage, W.R.: Complex Variables and the Laplace Transform for Engineers. Dover Publications, New York (1980)

48. El-Khazali, R., Batiha, I.M., Momani, S.: Approximation of fractional-order operators. In: Agarwal, P., Baleanu, D., Chen, Y., Momani, S., Machado, J., (Eds.): Fractional Calculus. ICFDA 2018. Springer, Singapore, pp. 121–151 (2019)

49. Abate, J., Whitt, W.: A unified framework for numerically inverting laplace transforms. INFORMS J. Comput. 18(4), 408–421 (2006)